Graphene enhances the proton selectivity of porous membrane in vanadium flow batteries

CrossMark

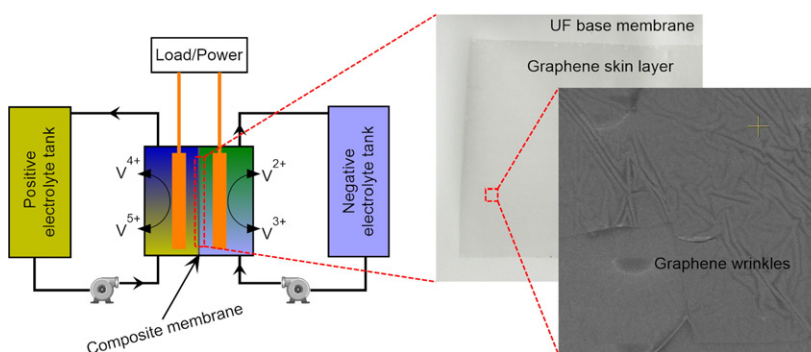Qing Chen [a], Yu-Yu Du [a], Kai-Min Li [a], Hui-Fang Xiao [a], Wei Wang [b],*, Wei-Ming Zhang [a],*

[a] College of Chemistry & Materials Engineering, Wenzhou University, Wenzhou 325000, China
[b] Ningbo Institute of Materials Technology & Engineering, Chinese Academy of Sciences, Ningbo 315201, China

HIGHLIGHTS

- A novel complex membrane is designed and fabricated to improve the vanadium flow battery performance;
- The complex membrane employs PES ultrafiltration membrane as support and graphene as proton-selection layer;
- The proton selectivity of membrane is significantly enhanced and the overall battery efficiencies are improved by 5-10%.

GRAPHICAL ABSTRACT

ABSTRACT

The vanadium flow battery (VFB) is one of the most promising technologies for large-scale energy storage, which has an enormous advantage in the stabilization and smooth output of renewable energy. As an essential separator in VFB, nanoporous membrane plays a key role in the final electrochemical performance, which requires both high H^+ conductivity and low vanadium permeability. In this work, a novel graphene enabled porous membrane material has been successfully designed and fabricated by directly transferring several layers of graphene onto the surface of traditional polyethersulfone ultrafiltration membrane. The experimental results show that the graphene layers will impact the composite membranes performance in batteries. After three graphene single layers attached, the proton selectivity of membrane is significantly enhanced, and the overall battery efficiencies are improved by 10% at 20 mA cm^{-2}. Therefore, attaching graphene layers is a feasible and promising strategy to improve the performance of nanoporous membrane in VFB applications.

© 2016 Elsevier Ltd. All rights reserved.

1. Introduction

The vanadium flow battery (VFB) is one of the most promising technologies for large-scale energy storage, which is necessary to integrate intermittent renewable energy seamlessly with the current electricity grid [1,2]. VFB operates on the electrochemical reactions of vanadium ions only (VO_2^+/VO^{2+} and V^{3+}/V^{2+}) in acidic aqueous solution [2]. A membrane separator is essential in VFB to separate positive and negative electrolytes and meanwhile capable of transferring ions (typically H^+) from one end to the other. An ideal membrane for VFB should exhibit a high H^+ conductivity to minimize the internal energy losses, a low permeability of vanadium ions to minimize self-discharge, and a

* Corresponding authors.
E-mail addresses: wangwei@nimte.ac.cn (W. Wang), weiming@iccas.ac.cn (W.-M. Zhang).

good chemical stability for long cycle life [3–5]. Currently in commercial systems and most research setups, the sulfonated fluorocarbon polymer Nafion (DuPont) is widely used as the best available membrane because of the excellent H$^+$ conductivity and chemical stability [5,6]. However, the extremely high cost and low ion selectivity (high vanadium crossover) hinder its large-scale applications [4,5,7]. Tremendous efforts have been made to search for alternative membrane materials, and most work is focused on cost-effective non-fluorinated polymer ion exchange membranes [8–10]. However, their oxidation stability needs to be further improved [4]. Recently, nanofiltration (NF) membranes are successfully used in VFB [11], which utilizes tiny pores to sieve H$^+$ and vanadium ions in nanoporous membranes instead of ion exchange groups in dense membranes. The radius of hydrated vanadium ion is much bigger, and the charge density of vanadium ion is higher than that of H$_3$O$^+$, so it is feasible to selectively transfer protons in the nanoporous membrane [11]. Unfortunately, the pore size distributions of conventional polymer based membranes are usually too wide and further surface modifications are needed to increase the H$^+$ selectivity. Some interesting modifications have been done on polyacrylonitrile (PAN) [11,12], polyethersulfone (PES) [13,14] and polyvinylidene fluoride (PVDF) [15] based membranes, and the overall battery performances are improved consequently.

In recent years, graphene has been increasingly explored as an excellent platform to develop size-selective molecular separation membrane [16–19]. Graphene-based membranes are ideal for selective molecular separation because of their atomic thickness (potential to maximize permeate flux) and excellent stability (mechanical robustness and chemical inertness) [18]. In addition, well-defined pores with extremely narrow size-distribution can be introduced into graphene by natural defects [20,21] or subsequent chemical modification [19,22,23] to further guarantee the high molecular selectivity. Solid works have confirmed that graphene-based membranes are much more selective and permeable than state-of-art polymeric membranes in water desalination [19], gas separation [16] and ion sieving [17,23]. A perfect graphene sheet is generally considered impermeable to all atoms and molecules [24]. However, a very recent work indicates that pristine graphene is actually highly permeable to protons, and the details of the transport process is intriguing [25]. Therefore, in combination with their mechanical robustness and chemical inertness, graphene-based membranes are promising candidates in many hydrogen-based technologies, including VFBs.

Pure graphene sheets are electron conductors and not able to prevent electric contact of the electrodes [3]. One effective solution is to combine graphene with a membrane which can provide electric insulation and mechanic supporting. PES membrane is widely used for ultrafiltration in water treatment and the porosity and morphology can be tuned easily [26]. Furthermore, its chemical stability in VFB system has been well validated [13,14,27]. All these features make PES membrane a natural choice of matrix when composited with graphene "skin layers". In the current work, a novel graphene/PES membrane is successfully designed and prepared, which employs PES ultrafiltration membrane as base matrix and graphene flakes as proton-selection layer. The preliminary tests indicate that the addition of graphene layers does enhance the membrane proton selectivity, as well as the overall battery performances. The results are very valuable for the graphene application in VFBs.

2. Materials and methods

2.1. Fabrication of graphene/PES membranes

The nanoporous membrane used in this study is UH004 tight ultrafiltration (UF) membrane (from MICRODYN-NADIR GmbH, Germany). The molecular weight cut-off (MWCO) is 4000 Da. The membrane consists of porous non-woven fabrics support and PES layer with permanently hydrophilic treatment. This hydrophilic membrane is

chemically stable, and can operate in the pH range of 0–14 below 95 °C in aqueous solutions.

In a typical fabrication process, copper foil (Cu, 99.99%) in size of 7×20 cm^2 was loaded in a tube furnace at 10 Pa and then heated to 1000 °C within 2 h with 8 sccm H$_2$ gas. After annealing Cu foil at 1000 °C for additional 30 min, 24 sccm CH$_4$ was introduced into the tube furnace for CVD growth of graphene film for the following 30 min. The graphene on Cu foil could be collected after cooling the furnace to room temperature. The graphene film was then transferred to UH004 membrane with the help of thermal release tape as in previous report [28]. Basically, it includes three steps. First, the graphene on Cu foil was attached to one piece of thermal release tape by a roll-to-roll machine. Subsequently, it was immersed in 0.1 M ammonium peroxydisulfate solution for etching Cu foil. Finally, the graphene film could be transferred to the UH004 membranes after a roll-to-roll thermal releasing process at 120 °C. In this work, different layers (1, 2 and 3 layers) of graphene were transferred separately onto the smooth surface (the skin layer side) of UH004 membranes, and then the composite graphene membranes with 1, 2 and 3 graphene layers were produced successfully.

2.2. Membrane characterizations

2.2.1. Membrane morphology

The cross-section morphology of UH004 base membrane was characterized by scanning electron microscope (SEM, JEOL SM-6700F, Japan). The surface morphologies of composite graphene membranes were recorded by optical camera as well as SEM (FEI Nova NanoSEM 200, America).

2.2.2. Membrane resistance

The area resistances of composite membranes were measured in a home-made electrochemical cell (Fig. 4a) according to the literature [12]. The cell was separated into two compartments and filled with 0.50 M H$_2$SO$_4$. The effective area of membrane (S) is 0.50 cm^2 in all tests. The area resistance of a membrane (r) is determined by the following equation:

$$r = (r_\mathrm{m} - r_0) \times S \tag{1}$$

where r_0 and $r_\mathrm{m.}$ represent the electric resistance of the cell without and with a membrane respectively. All cell resistances were obtained by electrochemical impedance spectroscopy (EIS, CHI 760E potentiostat, China) at a frequency range from 100 kHz to 100 Hz. The temperatures of H$_2$SO$_4$ solutions were maintained at 25 °C in all tests.

2.2.3. Transport numbers

The static state transport numbers of the composite graphene membranes were measured in a home-made cell (Fig. 5a) according to membrane potential [29,30]. The membrane was sandwiched in a cell filled with 0.20 M and 0.10 M HCl (or KCl) respectively, and the potential difference between the two Ag/AgCl electrodes was recorded. The cation transport number (t_+) is calculated by the following equation [30]:

$$t_+ = \frac{E_\mathrm{m}}{2E_0} \tag{2}$$

where E_m is the potential difference between the two electrodes, and E_0 is 16.08 mV. The operating temperatures were maintained precisely at 25 °C, and all membranes were immersed in 0.15 M HCl or KCl for at least 12 h for equilibrium before all tests.

2.2.4. Vanadium/proton permeability

The permselectivity between proton and vanadium ion was tested in a diffusion cell (Fig. 6a) similar to previous work [11,12]. Initially the left cell was filled with 50 mL of 1.0 M VOSO$_4$ and 2.0 M H$_2$SO$_4$, and the right

cell was filled with 50 mL of deionized water. Solutions in both cells were circulated by a peristaltic pump at a flow rate of 30 mL min^{-1}. Samples from the right cell were collected at a time interval of 20 min. The concentrations of H$^+$ were determined by automatic potentiometric titration (sample volume 1.0 mL or 0.50 mL, by INESAZDJ-4B automatic titrator). The concentrations of VO^{2+} were analyzed by a UV–vis spectrophotometer (Shimadzu UV-2450), and all samples were returned to the right cell immediately after the measurement. The H/V selectivity is defined by the following equation [12]:

$$\text{H/V selectivity} = \frac{\text{H}^+ \text{permeation rate}}{\text{VO}^{2+} \text{permeation rate}} \qquad (3)$$

2.3. Membrane evaluation in VFB battery

2.3.1. VFB battery performance

All of the VFB battery experimental tests were performed on a homebuilt setup containing 4–8 cells, as Fig. 1 shows. The VFB single cell was constructed by sandwiching a membrane with two carbon felt electrodes (effective area of 12 cm^2, original thickness of 6 mm before and 3.8 mm after clamping), and then clamped by two graphite plates as current collectors. The adhesion of graphene film is not an issue here, because the graphene "skin layer" was tightly clamped by the UF base membrane and carbon felt. Particularly, the composite membrane was mounted in a manner that the graphene "skin layer" is adjacent to the negative chamber (similar to that in Fig. 5a). The graphene film is completely protected against oxidation by VO$_2^+$, which guarantees the integrity of graphene films during the charge-discharge tests. The negative and positive electrolytes were 13.0 mL 1.5 M V^{2+}/V^{3+} in 3.0 M H$_2$SO$_4$ and 13.0 mL 1.5 M VO^{2+}/VO$_2^+$ in 3.0 M H$_2$SO$_4$ solutions respectively. Both electrolytes were continuously purged with argon during all tests. The electrolytes were circulated through the corresponding electrodes at a flow rate of 10 mL min^{-1} (flow velocity was 0.37 cm s^{-1} according to the cell geometry). Charge–discharge tests were conducted by a battery test system (LAND CT2001A, China) with current densities of 10–80 mA cm^{-2}. The cut-off cell voltages were set as 1.70 V and 0.80 V.

2.3.2. Self-discharge characterization

The self-discharge of VFB will result in decrease of open circuit voltage (OCV), so the curves of OCV decay are usually utilized to indicate the degree of battery self-discharging. The VFB single cell and electrolytes used here were identical with that in test of VFB battery performances above. Self-discharge tests began at the capacity of 300 mAh, namely the state of charge (SOC) of about 60%. OCV was recorded with battery test system (LAND CT2001A) until it dropped to 0.80 V.

3. Results and discussion

3.1. Morphologies of composite membranes

Fig. 2 presents optical photographs of the resulted graphene/UH004 composite membranes with one (Fig. 2a), two (Fig. 2b) and three (Fig. 2c) layers of graphene. The graphene layers are nearly transparent (transmittance >90%) [31], but they are still visible especially on smooth and white substrates. The detailed surface morphologies of the composite membranes are further characterized by SEM (Fig. 3). Fig. 3a shows the bare skin surface of UH004 membrane, which is quite smooth and clean in appearance. The cross-sectional SEM images of UH004 membrane are presented in Fig. S1 in Supplementary Materials. This membrane has a typical asymmetric structure, which consists of a nonwoven fabrics support layer, a very porous sponge layer with plenty of finger-like macropores, and a relative dense and smooth skin layer. The selectivity of the composite membrane is all contributed by the PES skin layer, which has a thickness of 10 μm (Fig. S1b). Meanwhile the smoothness of this skin layer provides enough adhesion strength to graphene layers, which enables a perfect transfer of graphene film from Cu foil to the base membrane. After introducing graphene onto the UH004 membrane, as shown in Fig. 3b–d, clear wrinkles can be observed on all the samples, which are originated from the graphene layers on top because of the differences of thermal expansion coefficients between graphene and copper [31]. These characteristic wrinkles are clearly visible in all SEM images, which definitely validate the perfect transfer of graphene layers onto the base membranes. Furthermore, a close-up view of the composite membrane with two layers of graphene is shown in Fig. 3e, in which the boundary of the top graphene layer as well as wrinkles of both layers are sharp and clear. The morphology characterizations by optical camera and SEM prove in concert that well-defined composite graphene membranes are obtained in this work.

3.2. Membrane resistance and ion selective permeability

The area resistance of membrane is critical in VFB applications, which determines the ohmic drop across the membrane and influences the overall battery performance. It was measured in a home-made electrochemical cell (Fig. 4a), and typical measured impedance spectra are shown in Fig. S2. Electric resistances of the cell without (r_0) and with a membrane (r_m) were determined according to other literature [14], and the area resistance (r) is calculated by Eq. (1). The corresponding results are shown in Fig. 4b, in which the error bars come from three independent tests (different membranes). The area resistance of UH004 base membrane is 0.81 Ω cm^2. The attachment of one single graphene layer significantly increases the area resistance of the membrane to 1.65 Ω cm^2. This phenomenon is straightforward because the attached

Fig. 1. (a) Experimental setup for VFB battery performance evaluation. (b) A close look of the VFB single cell.
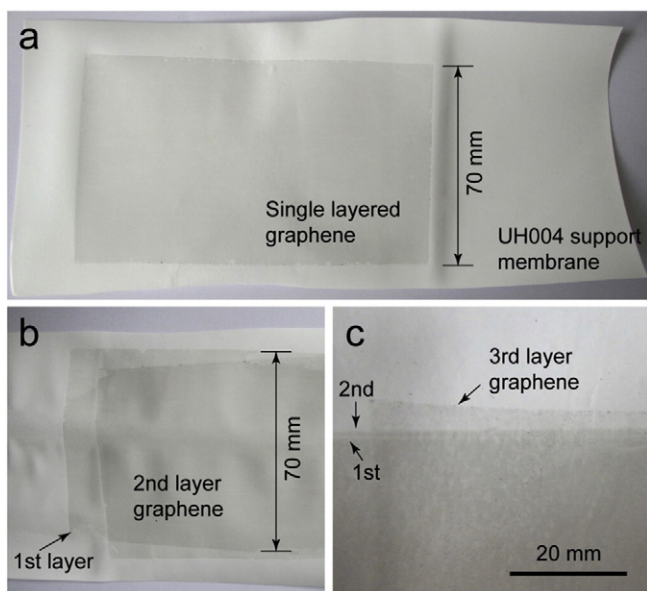
Fig. 2. Photographs of the graphene/UH004 membranes with one (a), two (b) and three (c) graphene layers.

Fig. 4. (a) The illustration of home-made cell for measuring membrane resistance. (b) The area resistance of prepared composite membranes.

graphene film brings about an extra obstacle in ion migrations. It is worth noting that the area resistance of single graphene layer can be estimated from this increment, namely 0.84 Ω cm^2. Hu and co-workers in Geim's laboratory have already investigated the proton transport through one-atom-thick crystals such as graphene [25]. Their results indicate that the area resistance of graphene monolayer is about 500 Ω cm^2 at 25 °C (i.e. area conductance of 2 mS cm^{-2}, much higher than our results), and reduces to 1.0 Ω cm^2 when the temperature increases to 110 °C [25]. The exact reason causing this inconsistency remains to be understood, while the following factors may be considered. First, the H$^+$ concentration is much different between the two tests. Hu et al. used a device placed inside a chamber filled with pure water (to provide
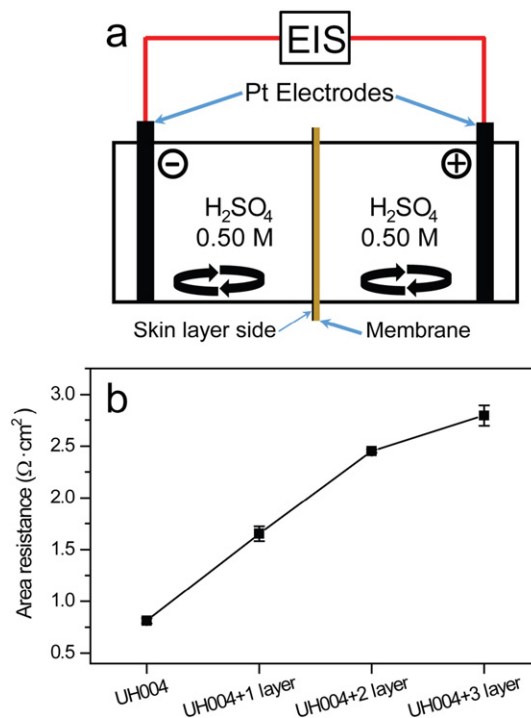
humidity) and forming gas (10% H$_2$ in Ar) [25]. Such parameters are designed for mimicking hydrogen fuel cell. Differently, 0.50 M H$_2$SO$_4$ was used in our electrochemical cell, which means that the H$^+$ concentration is much higher in the current work. It is well known that the area resistance of membrane increases inversely with ion concentration in supporting solution [32]. For example, the area resistances of commercial Selemion CMV membrane are 3 Ω cm^2 and 205 Ω cm^2 in 0.50 M and 0.020 M NaCl solutions, respectively [32]. Therefore, the greatly
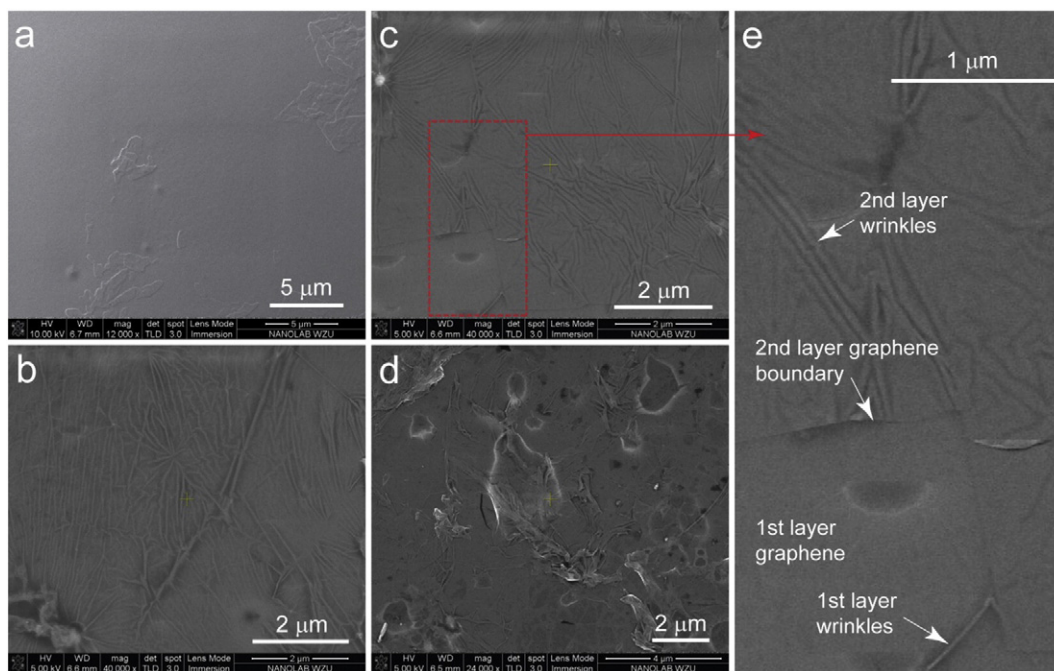

Fig. 3. Surface morphology images of the composite membranes obtained by SEM. (a) Bare surface of UH004 support membrane, and graphene/UH004 membrane with (b) one, (c) two and (d) three layers of graphene, respectively. (e) A close-up view of the composite membranes with two graphene layers, in which the wrinkles and boundaries of graphene layers are distinguishable.

different H$^+$ concentration could be the first reason. Second, there are more structure defects in our graphene film. Although high-quality single-layer graphene films can be deposited on Cu foils, structural defects and grain boundaries are unavoidable during the CVD process [20,31]. For example, pseudoperiodic corrugations and vacancies are found when graphene is grown on Cu (111) surface [20]. On the contrary, Hu and co-workers used perfect graphene without defects which was obtained by micromechanical cleavage [25]. Third, macroscopical cracks or tears are present in the current research. Cracks and wrinkles are readily observable on CVD graphene [31], and the integrity of graphene film may be further injured during the transfer process (Fig. 3e). So perhaps it is not surprising to observe a much lower area resistance for graphene single layer in our work. Fortunately it is advantageous for the composite membrane because high area resistance is not favored in VFB applications. It's noteworthy that the area resistances increase further after more graphene layers transferred, which are 2.45 Ω cm^2 and 2.80 Ω cm^2 for composite membranes with two and three graphene layers respectively.

Ion selective permeability is another key parameter for membrane separator in VFB applications. Ideal membranes for VFB should exhibit high permeability of proton (to minimize the internal energy loss) and low permeability of other ions (such as vanadium ions to minimize self-discharge) [3–5]. In other words, high proton selectivity is another desired feature besides low area resistance. The transport number is usually used to measure the permselectivity of counter-ions (charge carriers) through traditional ion exchange membrane [29,30], and this concept can be borrowed to evaluate the permselectivity of protons (or other cations) for our composite membranes. The cation transport numbers are measured in a home-made electrochemical cell (Fig. 5a) and the corresponding results are presented in Fig. 5b. It is found that the cation transport numbers in KCl solutions are highly low (0.531–0.570), and the anion transport numbers (1-t_+) are very close. These results indicate that the graphene/UH004 composite membranes have little permselectivity to K$^+$ or Cl$^-$ in KCl solutions (only slightly K$^+$ selective). However, the cation transport numbers in HCl solutions are reasonably high. The bare UH004 base membrane has a transport number of 0.917 in HCl solution (H$^+$ selective). This outstanding proton
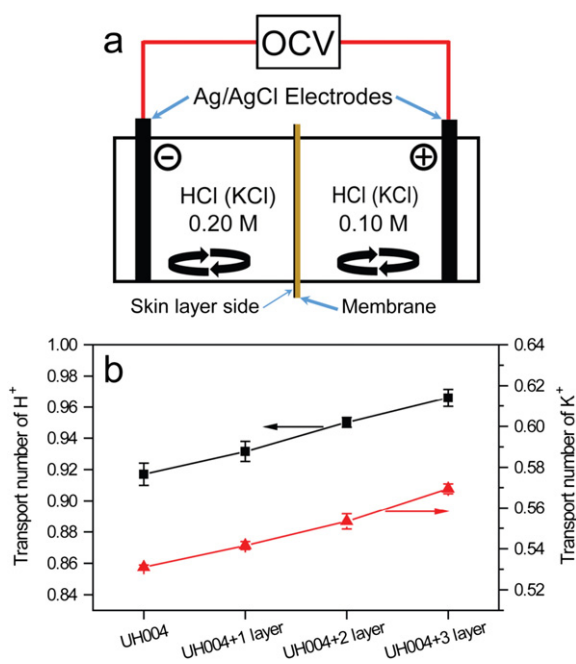
permselectivity is not surprising, since the ion mobility of H$^+$ is much higher than that of other ions (such as Cl$^-$) in the aqueous solutions, and the hydrated radii of protons are much smaller than other ions, which means it's much easier to permeate through nanopores in skin layer of UH004 membrane. Interestingly, the proton transport numbers of composite membranes increase proportionally after graphene layers being attached, which are 0.932, 0.950 and 0.966 for one, two and three graphene films respectively. The anion transport numbers (namely 1-t_+), which represent the fraction of the total current undertaken by Cl$^-$ in HCl solution, decrease greatly from 0.083 (without graphene) to 0.034 (with three graphene layers).

H/V selectivity is also an important index for measuring the H$^+$ permeability over other cations (vanadium ions) in VFB [11,12]. The diffusion cell (Fig. 6a) used for H/V selectivity measurement is similar to that in literature [12], and typical plots of VO^{2+} and H$^+$ concentrations in the water side are shown in Fig. S3. All membranes exhibit a much higher permeation rate for H$^+$ than that of VO^{2+}, which is given by the slope of corresponding plot. The resulted H/V selectivity is calculated by Eq. (3) and shown in Fig. 6b, in which the error bars come from three independent tests of different membrane samples. It is clearly shown that the H/V selectivity of composite membrane increase proportionally along with the graphene layers' number (from 24.8 without graphene, to 48.0 with 3 graphene layers). The result here well accords with the proton transport number evaluations in HCl solution above, which strongly indicates that attaching graphene layers onto the surfaces of nanoporous base membranes can enhance their proton permselectivity. As a result, the high proton permselectivity could lead to better battery performance in VFB applications.

3.3. VFB battery performance

Fig. 7 shows the charge–discharge curves of VFB single cells assembled with different composite graphene membranes at a current density of 80 mA cm^{-2}. The charge–discharge overpotential for all membranes are similar, which indicates that the voltage efficiencies (VE, defined as the ratio of discharge voltage divided by charge voltage) are highly close for cells with different composite membranes. The charge/discharge capacities are also available from these plots, and the Coulombic efficiency (CE, defined as the ratio of discharge capacity divided by charge capacity) can be readily calculated.

Self-discharge tests of VFB single cells are also carried on to further investigate the vanadium ions cross-over across the corresponding composite membranes. As shown in Fig. 8a, the OCV of VFB cell with bare UH004 membrane lasted about 8.0 h before it decreases rapidly
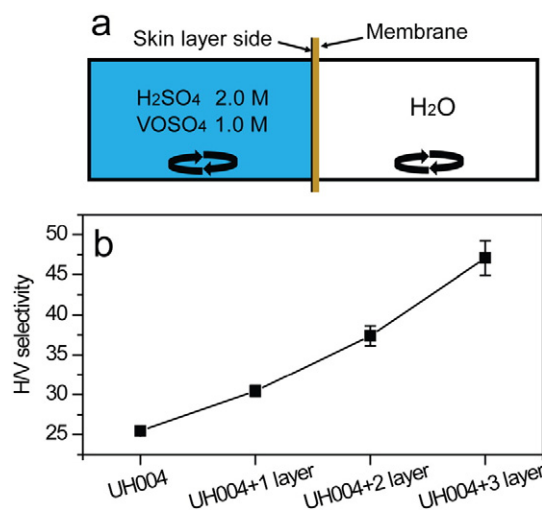

Fig. 5. (a) The illustration of home-made cell for measuring cation transport numbers (static state) in HCl or KCl solutions. (b) The H$^+$ and K$^+$ transport numbers of prepared composite membranes.

Fig. 6. (a) The diffusion cell used for measuring H/V selectivity. (b) The H/V selectivity of prepared composite membranes.
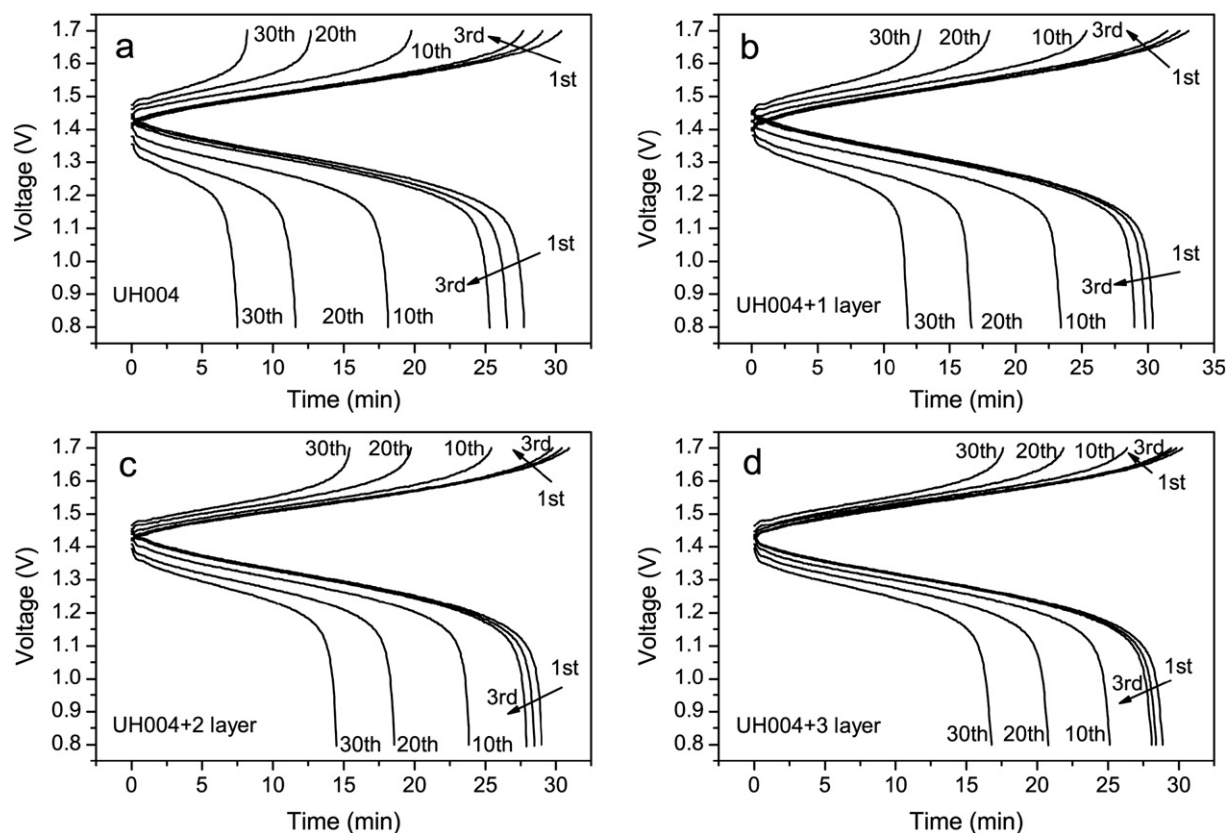
Fig. 7. Charge–discharge curves of VFB single cells with (a) bare UH004 base membrane, and attaching (b) one, (c) two and (d) three graphene layers at a current density of 80 mA cm^{-2} (960 mA for the cell).
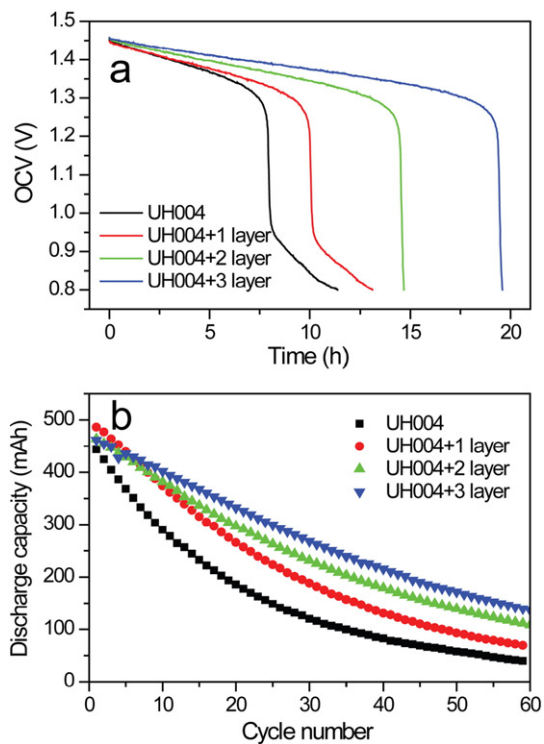

Fig. 8. (a) Self-discharge curves of VFB single cells with graphene composite membranes at an initial SOC of 60%. (b) The discharge capacity decay of VFB single cells with different composite graphene membranes at a current density of 80 mA cm^{-2}.

from 1.25 V to 0.95 V. After one, two and three graphene layers are attached, the corresponding OCV decay rates are lowered and the OCV time increases to 10.0 h, 14.6 h and 19.5 h respectively. These results are in accord with the VO^{2+} permeation rates in Fig. S3. The low cross-over rate of vanadium ions should be helpful to retain the capacity during the charge–discharge cycling. The discharge capacity decay of VFB cells with different membranes is shown in Fig. 8b. It manifests that the decay rate is lowered monotonously after graphene layers are attached. The results of OCV and capacity decay tests further confirm that the graphene layers hinder the vanadium ion cross-over in VFB applications.

More charge–discharge tests at different current densities (10–80 mA cm^{-2}) are carried on for all composite membranes, and the corresponding CE and VE values are plotted in Fig. 9. Furthermore, the energy efficiency (EE) of VFB single cell, which is defined as product of CE and EE, is also plotted in Fig. 9. For every cell with the same membrane, the CE increases while the VE decreases as the current density increases from 10 to 80 mA cm^{-2}. The maximum EE appears at about 40–50 mA cm^{-2}. The tendencies are similar to that of traditional ion exchange membrane (such as Nafion) used in VFB. The same data of efficiencies (Fig. S4) are rearranged to compare the battery performances of different membranes at the same current densities. It is clearly demonstrated that extra graphene layers increase the CE at all current densities, and the increment is more obvious for low current densities (12% at 10 mA cm^{-2}, and 3.6% at 80 mA cm^{-2}). This phenomenon is reasonable because extra graphene layers hinder the permeation of vanadium ions (causing capacity lost) during the charge–discharge process. However, the VE is very stable at nearly all current densities, and the mechanism is more complicated. Firstly, the area resistance increases after graphene layers transferred, which will decrease the VE. While on the other hand, proton selectivity is
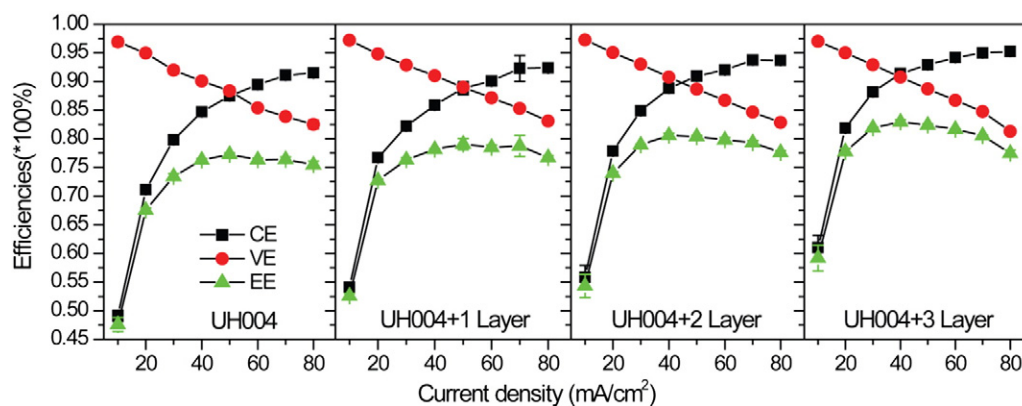
Fig. 9. VFB single cell performances of composite membranes at different current densities (10–80 mA cm^{-2}). CE, Columbic efficiency; VE, voltage efficiency; EE, energy efficiency.

significantly improved because of the graphene layers, and this will increase the VE. The improved proton selectivity counteracts the increased area resistance, and stabilizes the VE of composite membranes with more graphene layers. It is worth noting that the area resistance impacts more at higher current densities, and a slight decrease of VE is observed at 80 mA cm^{-2} (right panel in Fig. S4). The stable VE and increased CE cause incremental EE at nearly all current densities, which are also shown in Fig. S4. It indubitably shows that attaching graphene layers is a feasible and promising strategy to improve the EE of nanoporous membrane. For pristine graphene films, the area resistance is still too high (~0.8 Ω cm^2 for single-layer graphene), so the improvement is more obvious at low current densities. The EE are improved by 10% and 5.2% at 20 and 60 mA cm^{-2} respectively.

Additionally, the graphene enabled membranes show reasonable stability in this work. Each membrane was tested for at least 200 cycles (the electrolytes were changed for several times) and no obvious performance degradation was observed. Creating well-defined pores with extremely narrow size distribution on graphene, or simply increasing the operating temperature of VFB, could be helpful to decrease the area resistance while keeping the proton selectivity. Maybe further efforts can be made to increase the overall performance of composite graphene membranes.

4. Conclusions

In the current work, novel graphene/UH004 composite membranes are fabricated by transferring graphene layers onto UH004 base membranes. The extra graphene as "skin layer" increases the overall area resistance of membrane, which can effectively hinder ions in electrolytes, especially the vanadium ions, from permeating across the membranes. With the significantly reduced vanadium cross-over, CE succeeds a large improvement. Furthermore, these graphene layers also greatly increase the proton selectivity, which is proven by the investigations of proton transport number as well as H/V selectivity. Detailed electrochemical characterization shows that the improved proton selectivity counteracts the increase of area resistance and stabilizes the VE for all composite membranes. The stable VE and increased CE bring significant improvement of overall battery performance, and the EE increases by 10% and 5.2% at 20 and 60 mA cm^{-2}, respectively, after three graphene single layers are attached. In addition, the capacity decay is also relieved. Adding more graphene layers (>3) will further improve the overall battery efficiencies at low current densities but not at high current densities, because a trade-off exists between selectivity and electrical resistance. In the final analysis, the results here show that the introduction of graphene layers onto nanoporous membrane is a feasible and promising strategy to improve the overall performance in VFB applications.

Appendix A. Supplementary data

Supplementary images including SEM images of the base membrane, measured impedance spectra, VO^{2+}/H$^+$ permeation rates, and battery performances. Supplementary data associated with this article can be found in the online version, at doi: http://dx.doi.org/10.1016/j.matdes.2016.10.019.

References

[1] J. Rugolo, M.J. Aziz, Electricity storage for intermittent renewable sources, Energy Environ. Sci. 5 (2012) 7151–7160.
[2] Z. Yang, J. Zhang, M.C.W. Kintner-Meyer, X. Lu, D. Choi, et al., Electrochemical energy storage for green grid, Chem. Rev. 111 (2011) 3577–3613.
[3] P. Arora, Z. Zhang, Battery separators, Chem. Rev. 104 (2004) 4419–4462.
[4] X. Li, H. Zhang, Z. Mai, H. Zhang, I. Vankelecom, Ion exchange membranes for vanadium redox flow battery (VRB) applications, Energy Environ. Sci. 4 (2011) 1147–1160.
[5] B. Schwenzer, J. Zhang, S. Kim, L. Li, J. Liu, et al., Membrane development for vanadium redox flow batteries, ChemSusChem 4 (2011) 1388–1406.
[6] S. Eckroad, Vanadium Redox Flow Batteries: An In-Depth Analysis, Electric Power Research Institute (EPRI), Palo Alto, CA, 2007.
[7] C. Ding, H. Zhang, X. Li, T. Liu, F. Xing, Vanadium flow battery for energy storage: prospects and challenges, J. Phys. Chem. Lett. 4 (2013) 1281–1294.
[8] Z. Mai, H. Zhang, X. Li, C. Bi, H. Dai, Sulfonated poly(tetramethydiphenyl ether ether ketone) membranes for vanadium redox flow battery application, J. Power Sources 196 (2011) 482–487.
[9] Z. Xia, S. Yuan, G. Jiang, X. Guo, J. Fang, et al., Polybenzimidazoles with pendant quaternary ammonium groups as potential anion exchange membranes for fuel cells, J. Membr. Sci. 390–391 (2012) 152–159.
[10] D. Chen, M.A. Hickner, E. Agar, E.C. Kumbur, Optimized anion exchange membranes for vanadium redox flow batteries, ACS Appl. Mater. Interfaces 5 (2013) 7559–7566.
[11] H. Zhang, H. Zhang, X. Li, Z. Mai, J. Zhang, Nanofiltration (NF) membranes: the next generation separators for all vanadium redox flow batteries (VRBs)? Energy Environ. Sci. 4 (2011) 1676–1679.
[12] H. Zhang, H. Zhang, X. Li, Z. Mai, W. Wei, Silica modified nanofiltration membranes with improved selectivity for redox flow battery application, Energy Environ. Sci. 5 (2012) 6299–6303.
[13] Y. Li, H. Zhang, X. Li, H. Zhang, W. Wei, Porous poly (ether sulfone) membranes with tunable morphology: fabrication and their application for vanadium flow battery, J. Power Sources 233 (2013) 202–208.
[14] Y. Li, X. Li, J. Cao, W. Xu, H. Zhang, Composite porous membranes with an ultrathin selective layer for vanadium flow batteries, Chem. Commun. 50 (2014) 4596–4599.
[15] W. Wei, H. Zhang, X. Li, H. Zhang, Y. Li, et al., Hydrophobic asymmetric ultrafiltration PVDF membranes: an alternative separator for VFB with excellent stability, Phys. Chem. Chem. Phys. 15 (2013) 1766–1771.
[16] H.W. Kim, H.W. Yoon, S.-M. Yoon, B.M. Yoo, B.K. Ahn, et al., Selective gas transport through few-layered graphene and graphene oxide membranes, Science 342 (2013) 91–95.
[17] R.K. Joshi, P. Carbone, F.C. Wang, V.G. Kravets, Y. Su, et al., Precise and ultrafast molecular sieving through graphene oxide membranes, Science 343 (2014) 752–754.
[18] L. Huang, M. Zhang, C. Li, G. Shi, Graphene-based membranes for molecular separation, J. Phys. Chem. Lett. 6 (2015) 2806–2815.

[19] S.P. Surwade, S.N. Smirnov, I.V. Vlassiouk, R.R. Unocic, G.M. Veith, et al., Water desalination using nanoporous single-layer graphene, Nat. Nanotechnol. 10 (2015) 459–464.

[20] T. Niu, M. Zhou, J. Zhang, Y. Feng, W. Chen, Growth intermediates for CVD graphene on Cu(111): carbon clusters and defective graphene, J. Am. Chem. Soc. 135 (2013) 8409–8414.

[21] D. Van Lam, S.-M. Kim, Y. Cho, J.-H. Kim, H.-J. Lee, et al., Healing defective CVD-graphene through vapor phase treatment, Nanoscale 6 (2014) 5639–5644.

[22] K. Celebi, J. Buchheim, R.M. Wyss, A. Droudian, P. Gasser, et al., Ultimate permeation across atomically thin porous graphene, Science 344 (2014) 289–292.

[23] S.C. O'Hern, M.S.H. Boutilier, J.-C. Idrobo, Y. Song, J. Kong, et al., Selective ionic transport through tunable subnanometer pores in single-layer graphene membranes, Nano Lett. 14 (2014) 1234–1241.

[24] V. Berry, Impermeability of graphene and its applications, Carbon 62 (2013) 1–10.

[25] S. Hu, M. Lozada-Hidalgo, F.C. Wang, A. Mishchenko, F. Schedin, et al., Proton transport through one-atom-thick crystals, Nature 516 (2014) 227–230.

[26] C. Zhao, J. Xue, F. Ran, S. Sun, Modification of polyethersulfone membranes – a review of methods, Prog. Mater. Sci. 58 (2013) 76–150.

[27] W. Xu, X. Li, J. Cao, Z. Yuan, H. Zhang, Morphology and performance of poly(ether sulfone)/sulfonated poly(ether ether ketone) blend porous membranes for vanadium flow battery application, RSC Adv. 4 (2014) 40400–40406.

[28] S. Bae, H. Kim, Y. Lee, X. Xu, J.-S. Park, et al., Roll-to-roll production of 30-inch graphene films for transparent electrodes, Nat. Nanotechnol. 5 (2010) 574–578.

[29] T. Sata, Ion Exchange Membranes: Preparation, Characterization, Modification and Application, The Royal Society of Chemistry, Cambridge, 2004.

[30] T. Xu, H. Chuanhui, Preparation and Application of Ion Exchange Membranes, Chemical Industry Press, Beijing, 2008.

[31] C. Mattevi, H. Kim, M. Chhowalla, A review of chemical vapour deposition of graphene on copper, J. Mater. Chem. 21 (2011) 3324–3334.

[32] G.M. Geise, A.J. Curtis, M.C. Hatzell, M.A. Hickner, B.E. Logan, Salt concentration differences Alter membrane resistance in reverse electrodialysis stacks, Environ. Sci. Technol. Lett. 1 (2014) 36–39.